LETTERS

DNA-guided crystallization of colloidal nanoparticles

Dmytro Nykypanchuk[1]*, Mathew M. Maye[1]*, Daniel van der Lelie[2] & Oleg Gang[1]

Many nanometre-sized building blocks will readily assemble into macroscopic structures. If the process is accompanied by effective control over the interactions between the blocks and all entropic effects[1,2], then the resultant structures will be ordered with a precision hard to achieve with other fabrication methods. But it remains challenging to use self-assembly to design systems comprised of different types of building blocks—to realize novel magnetic, plasmonic and photonic metamaterials[3–5], for example. A conceptually simple idea for overcoming this problem is the use of 'encodable' interactions between building blocks; this can in principle be straightforwardly implemented using biomolecules[6–10]. Strategies that use DNA programmability to control the placement of nanoparticles in one and two dimensions have indeed been demonstrated[11–13]. However, our theoretical understanding of how to extend this approach to three dimensions is limited[14,15], and most experiments have yielded amorphous aggregates[16–19] and only occasionally crystallites of close-packed micrometre-sized particles[9,10]. Here, we report the formation of three-dimensional crystalline assemblies of gold nanoparticles mediated by interactions between complementary DNA molecules attached to the nanoparticles' surface. We find that the nanoparticle crystals form reversibly during heating and cooling cycles. Moreover, the body-centred-cubic lattice structure is temperature-tuneable and structurally open, with particles occupying only ~4% of the unit cell volume. We expect that our DNA-mediated crystallization approach, and the insight into DNA design requirements it has provided, will facilitate both the creation of new classes of ordered multicomponent metamaterials and the exploration of the phase behaviour of hybrid systems with addressable interactions.

Theoretical predictions indicate[15] that transitions to three-dimensional (3D) ordered phases from commonly observed disordered states[16–19] in a DNA-guided particle assembly can occur for particular shapes and ranges of interparticle interaction potentials, which are defined by the interplay of attraction and repulsion energies, E_a and E_r. The phase behaviour can be parameterized using E_a/E_r, and $\varepsilon = d_r/d_p$, which represents a relative range of repulsive interactions d_r with respect to particle size d_p (ref. 15). These parameters in DNA particle assembly systems can be conveniently controlled in a variety of ways, including the design of individual DNA, DNA shell structure and solution ionic strengths[20–23]. Experimentally, DNA-induced particle crystallization into random hexagonal close-packed crystals was observed near surfaces for single-component micrometre-sized particle systems with short-range interactions ($\varepsilon \rightarrow 0$)[9,10]. Particle crystallization with long-range interaction potentials ($\varepsilon \approx 1$) for which diverse non-close-packed structures are expected[15] (such as DNA-induced crystallization of nanoparticles) has not been achieved. Here we vary the length of the linking DNA molecules in the model DNA–nanoparticle system, providing a straightforward means of systematically changing the repulsive component of the interparticle potential.

Figure 1a and b shows a schematic illustration of the assembly system used to measure the effect of DNA structure on assembly long-range order, as studied under a variety of thermal conditions. In each assembly system, a set of DNA-capped gold nanoparticles (denoted A and B) with different DNA structures (Supplementary Table 1) were allowed to assemble by DNA hybridization into mesoscale aggregates (Fig. 1b, c). The complementary outer recognition sequences of the DNA capping provided the driving force for A and B particle assembly. The length of the recognition sequence, N_a, sets the scale of adhesion (per hybridized linker), $E_a \propto N_a$, to be from ~30 kT at room temperature (~25 °C) to ~0 kT at the DNA melting temperature T_m. Hence, E_a is approximately constant for all studied systems at any given temperature, with van der Waals interactions (<0.5 kT) contributing insignificantly[20,24]. In a ''brush'' regime, the length N of DNA and the flexibility of the non-complementary internal spacer allowed us to tune the range, $d_r \propto N^{3/5}$, of repulsive interaction and its strength $E_r \propto N^{3/5}/(N^{3/5} - cN_a)$, where c is defined by persistence length and molecule surface density and is constant for all studied systems[20,25]. For single-stranded DNA, experimentally relevant separations between particles, sufficient DNA surface densities and suitable salt concentrations, an estimated magnitude of E_r can reach several kT per chain[20]. Thus, the use of multiple systems with constant E_a (that is, recognition sequence), and varied d_r (that is, spacer lengths), enabled effective interparticle potential tuning, providing the environment required to achieve crystalline morphologies of nanoparticle assemblies via the thermal pathway shown in Fig. 1.

To monitor directly the *in situ* phase behaviour of the systems, we used synchrotron-based small-angle X-ray scattering (SAXS). The internal structure of the nanoparticle assemblies was investigated under different thermal conditions, including: assembly at room temperature; heating the assembly to pre-melting temperatures (T_{pm}) and DNA melting temperatures (T_m); and cooling the assembly below T_m. Figure 2 illustrates the observed scattering changes along this thermal pathway towards crystallization. The peak positions and relative heights in the SAXS patterns and in the extracted structure factors S(q) (see Methods and Supplementary Discussion and Supplementary Fig 1 and 2) reveal insights into the structure of the assemblies, while the number of peaks and their widths reflect the degree of ordering within the structure.

From the thermal cycling described, we found that systems IV and V, which have the longest flexible spacers (35 and 50 bases respectively), showed spontaneous crystalline organization with remarkable degrees of long-range order. In contrast, systems with shorter spacers (systems I–III) or more rigid spacers (see Supplementary Discussion and Supplementary Fig. 1) remained amorphous upon cooling. For the crystallizing system IV (Fig. 2), the ordered structure appears after melting and subsequent cooling below T_m at ~60 °C; this is signified by the emergence of several sharp diffraction peaks in the presence of strong diffuse scattering attributed to a large contribution by the nanoparticle's form factor. This suggests the presence

[1]Center for Functional Nanomaterials, [2]Biology Department, Brookhaven National Laboratory, Upton, New York 11973, USA.
*These authors contributed equally to this work.

of nuclei of the newly forming phase in coexistence with unassembled particles. Upon further cooling to 59–57 °C, we observed complete crystallization of the sample, indicated by the dramatic reduction of particle form factor and the presence of sharp circular patterns characteristic of un-oriented polycrystalline samples (that is, powder scattering). This crystalline formation occurred within only a few minutes, unaffected by the cooling rate available in our set-up (up to 1 °C min^{-1}). The observed crystallization is the result of specific DNA–DNA interactions, as confirmed by multiple control experiments with noncomplementary DNA-capped nanoparticles or with uncapped particles, none of which exhibit assembly. In addition, the DNA specificity of the assembled systems is manifested in melting profiles obtained with both ultraviolet–visible spectrophotometry (Supplementary Table S2) and SAXS for all systems.

The SAXS patterns in Fig. 3 reveals seven and ten orders of resolution-limited Bragg's peaks for systems IV and V, respectively, demonstrating their crystalline 3D structures, remarkable degrees of long-range ordering, and crystallite sizes of at least ~0.5 μm, as estimated from the scattering correlation length, $\xi \approx 2\pi/\Delta q$ (ref. 26), where Δq is the resolution-corrected ($\Delta q_{res} \approx 0.0015$ Å^{-1}) full-width at half-maximum (FWHM) of the first diffraction peak. Once formed, these crystalline structures were indeed reversible, as confirmed by multiple assembly–disassembly cycles, without a noticeable loss of ordering quality or changes in system behaviour or T_m. Analysis of the peak position ratios reveal $q_x/q_1 = \sqrt{1}:\sqrt{2}:\sqrt{3}:\sqrt{4}:\sqrt{5}:\sqrt{6}:\sqrt{7}$, which correspond to the $Im'3m$ space group, a body-centred cubic (b.c.c.) structure, as shown in Fig. 3a. The S(q) peak height also qualitatively follows the relative intensities predicted for b.c.c. arrangement. The observed b.c.c. structure meets the requirement for optimizing interaction energies in the studied binary AB system[15] (with AA and BB interactions being mainly repulsive), by having only particle B in the coordination shell of A and vice versa, thus forming CsCl-type superlattices.

The measured lattice parameters a for the observed b.c.c. structure are ~35 nm at 30 °C and ~42.4 nm at 28 °C for systems IV and V,

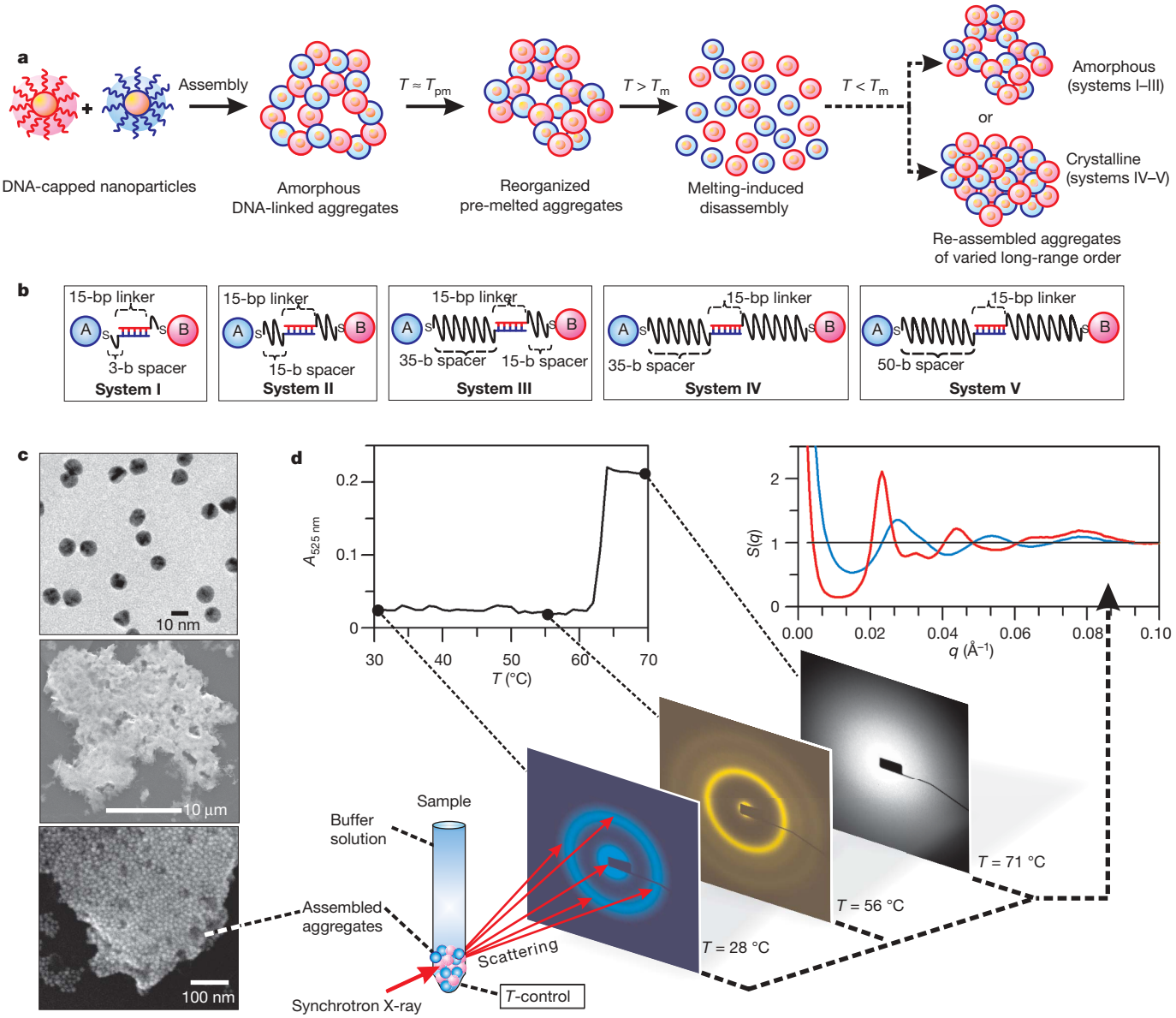

Figure 1 | Schematic of experimental design. a, The assembly system of DNA-capped nanoparticles, the aggregates of which show a series of structural changes under a variety of thermal conditions. **b**, DNA linkages between nanoparticles (one interparticle linkage is shown for clarity, not to scale) with recognition sequences for the A (blue) and B (red) sets of DNA capping. bp, base pairs. b, bases. s, thiol termination of DNA. **c**, Representative transmission (top) and scanning (middle, bottom) electron microscopy images of nanoparticles before (top) and after (middle, bottom) assembly at room temperature. **d**, Typical example of experimental measurements that reveal a correlation between the ultraviolet–visible melting profile of the aggregate and its internal structure as probed by *in situ* SAXS measurements at room temperature, pre-melting temperature, and above the disassembly/melting temperature.

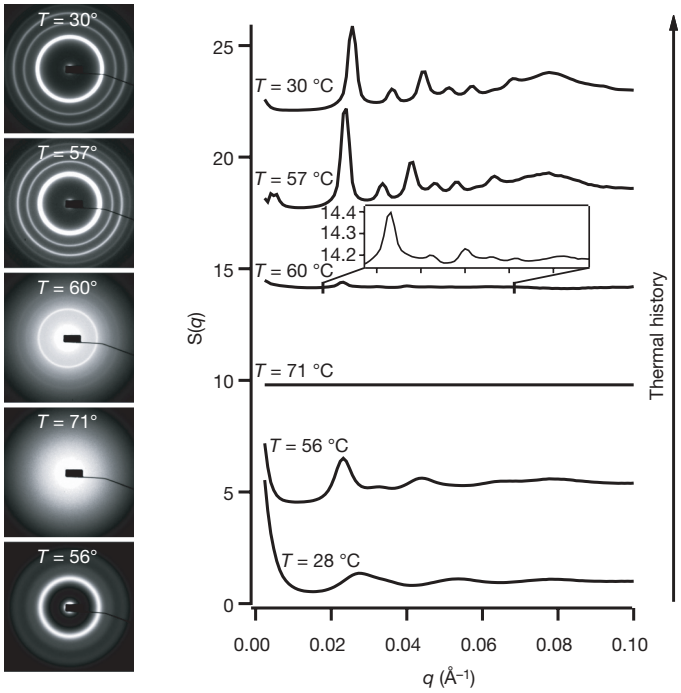

Figure 2 | Crystallization pathway for system IV. SAXS images and extracted structure factors S(q) for system IV as brought through a heating–cooling cycle for the temperatures shown (temperature stability ±0.1 °C) across the assembly melting point. S(q) lines are shifted consecutively by 4.4 units from each other. The inset shows the zoom-in area of S(q) at 60 °C for q ranging from 0.018 to 0.068 Å^{-1}.

respectively. At these a values, the particles are $d_1^{IV} = 18.9$ nm and $d_1^{V} = 24.2$ nm apart, in the first coordination shell of the obtained crystals, for systems IV and V, respectively, as calculated from a ($d_1 = \sqrt{3}/2a - d_p$). These values are close to the equilibrium linker dimensions, estimated from the scaling argument[27] for the DNA capping environment to be 18 and 23 nm. These a values indicate that the crystalline structures are remarkably open, in which nanoparticles occupy only ~2–4% of the volume and the DNAs occupy an additional 4–5%. Thus, more than ~90% of the assembled structure volume is occupied by solvent molecules, which is far higher than the typical void space in packed hard spheres in a b.c.c. orientation (~32%). Such open framework of a superlattice makes the structure vulnerable to collapse upon solvent removal, which prevents accurate morphology visualization by electron microscopy, but at the same time, makes the crystals highly accessible for modifications, molecular transport and storage. In addition, a was found to be highly sensitive to temperature and is primarily defined by thermal properties of DNA. A measured thermal expansion coefficient $\alpha \approx 3 \times 10^{-3}\,K^{-1}$ (Fig. 3b, c) for systems IV and V is two orders of magnitude larger than conventional materials, promising future functional tunability at convenient temperatures.

The requirement for thermal cycling across T_m for system crystallization indicates that formation of the DNA guided nanoparticle crystals is kinetically hindered at temperatures much below T_m. The particles are probably arrested in non-equilibrium positions due to local DNA crowding and high DNA hybridization energy, exceeding 30 kT for the used recognition sequences. Structurally, this may result in non-uniaxial DNA hybridization that provides linkages at the angle to the common axes between particles, leading to possibly shorter-than-equilibrium distances between particles and distance non-uniformity (that is, amorphousness). Heating the system to T_m reduces the DNA-induced attraction energy and allows the system to anneal towards equilibrium positions. The presence of the metastable state upon initial assembly at room temperature was experimentally confirmed by sharpening of the scattering peaks, the result of more-uniform spatial organization of particles, and the increase of interparticle distances upon annealing at T_{pm} values (see Supplementary Discussion). Interestingly, this ordering with temperature is more pronounced for systems with longer linkers and more flexible spacers (for systems IV and V). These more-flexible spacer structures allow for larger local rearrangements near T_m, that

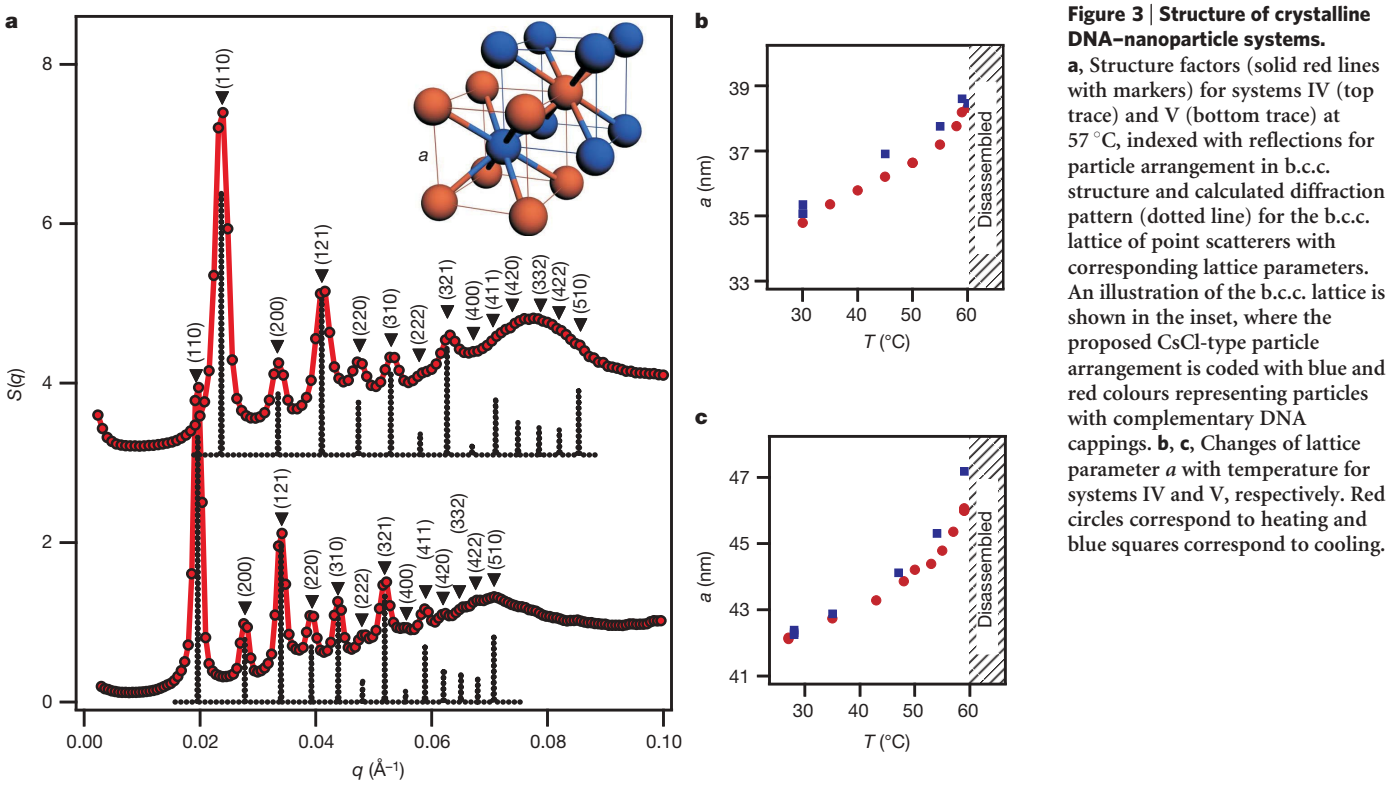

Figure 3 | Structure of crystalline DNA–nanoparticle systems. **a**, Structure factors (solid red lines with markers) for systems IV (top trace) and V (bottom trace) at 57 °C, indexed with reflections for particle arrangement in b.c.c. structure and calculated diffraction pattern (dotted line) for the b.c.c. lattice of point scatterers with corresponding lattice parameters. An illustration of the b.c.c. lattice is shown in the inset, where the proposed CsCl-type particle arrangement is coded with blue and red colours representing particles with complementary DNA cappings. **b**, **c**, Changes of lattice parameter a with temperature for systems IV and V, respectively. Red circles correspond to heating and blue squares correspond to cooling.

is, resulting in a lower energy penalty for deformation of DNA with a longer spacer by a given length, owing to the energy scaling with DNA size as $\sim(1-1/(bN^{3/5}))^{5/2}$, where b is a constant for all described systems and is determined by chain stiffness and DNA surface density[27,28]. In addition to facilitating pre-ordering below T_m, this lower penalty for DNA deformation helps particles 'squeezing' between neighbours to achieve optimal crystalline packing once bonds between particles become reversible at T_m.

The equilibrium state in the assembled system is also affected by linker structure as described above, through E_a/E_r and ε parameters. A quantitative comparison between theoretically predicted behaviour[15] and observed crystallization is problematic owing to the experimentally different realization of repulsion tuning, the influence of increased particle curvature on DNA behaviour, and effects associated with high local density of DNA chains. But qualitatively, the observed transition from disorder to b.c.c. phase occurs with increasing E_a/E_r parameter and ε close to unity—that is, at conditions similar to those predicted.

Our results show that DNA design has profound effects on the equilibrium state of the assembled systems, as well as on the kinetically favourable path to equilibrium. The proper equilibrium balance of repulsion and attraction energies of the system provides the possibility of forming ordered structures, and a smooth energy landscape, brought about by long flexible linkers and the described thermal pathway, provides the means to achieve this part of a phase space.

The thermodynamic stability and reversibility of the ordered assemblies, combined with the sensitivity of interparticle distances to biomolecular conformations and temperature, opens up new horizons for sensing, studies on biological interactions, and the tuneable functionality of metamaterials. Moreover, decoupling the assembly structure from the properties of nanoparticle constituents will allow for the incorporation of a broad variety of nanoscale objects in ordered 3D hybrid assemblies, the phases and behaviours of which are yet to be explored.

METHODS SUMMARY

Gold nanoparticles (11.4 ± 1.0 nm for systems I to IV and 12.5 ± 1.1 nm for system V) were synthesized as reported recently[16,17], and functionalized with a single-stranded DNA using methods to achieve high DNA coverage[29]. Thiol-modified single-stranded oligonucleotides (100–300 nmoles) were purchased as disulphides and reduced for 30 min with 0.1–0.3 ml of a 100 mM dithiothreitol solution in purified water or buffer before being purified with Sephadex columns. The total number of single-stranded DNAs bound to each particle was determined as $\sim 60(\pm 5)$ (~ 31.7 pmol cm^{-2}; ref. 30).

Particle assembly was carried out at 25 °C by combining equimolar amounts of type-A and type-B DNA-capped gold particles in 200 µl ([A] = [B] = ~30 nM) solution of 10 mM phosphate buffer, 0.2 M NaCl, pH = 7.1. The particles were allowed to assemble into aggregates overnight, and the resulting precipitate was collected and transferred in buffer to a quartz capillary (1.0 mm diameter), and sealed with wax.

SAXS experiments were performed at the National Synchrotron Light Source's X-21 beamline. The scattering data were collected with a charge-coupled device (CCD) area detector at wavelength $\lambda = 1.5498$ Å. The data are presented as the structure factor $S(q)$ versus scattering vector, $q = (4\pi/\lambda)\sin(\theta/2)$, where θ is the scattering angle. The values of q were calibrated with silver behenate ($q = 0.1076$ Å^{-1}). $S(q)$ was calculated as $I_a(q)/I_p(q)$, where $I_a(q)$ and $I_p(q)$ are background-corrected angular averaged one-dimensional scattering intensities for a system under consideration and un-aggregated system, respectively. The peak positions in $S(q)$ are determined by fitting a lorenzian form.

Ultraviolet–visible spectrophotometry spectra were collected on a Perkin Elmer Lambda 35 spectrometer. Melting analysis was performed in conjunction with a Perkin Elmer PTP-1 Peltier Temperature Programmer between 20–75 °C with a temperature ramp of 1 °C per min while stirring, in a solution of 10 mM phosphate buffer, 0.20 M NaCl, at pH = 7.1.

Received 5 July; accepted 21 December 2007.

1. Shevchenko, E. V., Talapin, D. V., Kotov, N. A., O'Brien, S. & Murray, C. B. Structural diversity in binary nanoparticle superlattices. *Nature* **439,** 55–59 (2006).
2. Zhang, H., Edwards, E. W., Wang, D. Y. & Mohwald, H. Directing the self-assembly of nanocrystals beyond colloidal crystallization. *Phys. Chem. Chem. Phys.* **8,** 3288–3299 (2006).
3. Lee, J., Hernandez, P., Lee, J., Govorov, A. O. & Kotov, N. A. Exciton–plasmon interactions in molecular spring assemblies of nanowires and wavelength-based protein detection. *Nature Mater.* **6,** 291–295 (2007).
4. Redl, F. X., Cho, K. S., Murray, C. B. & O'Brien, S. Three-dimensional binary superlattices of magnetic nanocrystals and semiconductor quantum dots. *Nature* **423,** 968–971 (2003).
5. Urban, J. J., Talapin, D. V., Shevchenko, E. V., Kagan, C. R. & Murray, C. B. Synergism in binary nanocrystal superlattices leads to enhanced p-type conductivity in self-assembled PbTe/Ag-2 Te thin films. *Nature Mater.* **6,** 115–121 (2007).
6. Katz, E. & Willner, I. Integrated nanoparticle-biomolecule hybrid systems: Synthesis, properties, and applications. *Angew. Chem. Int. Edn Engl.* **43,** 6042–6108 (2004).
7. Alivisatos, A. P. *et al.* Organization of 'nanocrystal molecules' using DNA. *Nature* **382,** 609–611 (1996).
8. Mirkin, C. A., Letsinger, R. L., Mucic, R. C. & Storhoff, J. J. A DNA-based method for rationally assembling nanoparticles into macroscopic materials. *Nature* **382,** 607–609 (1996).
9. Kim, A. J., Biancaniello, P. L. & Crocker, J. C. Engineering DNA-mediated colloidal crystallization. *Langmuir* **22,** 1991–2001 (2006).
10. Biancaniello, P. L., Kim, A. J. & Crocker, J. C. Colloidal interactions and self-assembly using DNA hybridization. *Phys. Rev. Lett.* **94,** 058302 (2005).
11. Pinto, Y. Y. *et al.* Sequence-encoded self-assembly of multiple-nanocomponent arrays by 2D DNA scaffolding. *Nano Lett.* **5,** 2399–2402 (2005).
12. Tang, Z. Y. & Kotov, N. A. One-dimensional assemblies of nanoparticles: preparation, properties, and promise. *Adv. Mater.* **17,** 951–962 (2005).
13. Zhang, J. P., Liu, Y., Ke, Y. G. & Yan, H. Periodic square-like gold nanoparticle arrays templated by self-assembled 2D DNA nanogrids on a surface. *Nano Lett.* **6,** 248–251 (2006).
14. Lukatsky, D. B., Mulder, B. M. & Frenkel, D. Designing ordered DNA-linked nanoparticle assemblies. *J. Phys. Cond. Matt.* **18,** S567–S580 (2006).
15. Tkachenko, A. V. Morphological diversity of DNA-colloidal self-assembly. *Phys. Rev. Lett.* **89,** 148303 (2002).
16. Maye, M. M., Nykypanchuk, D., van der Lelie, D. & Gang, O. A simple method for kinetic control of DNA-induced nanoparticle assembly. *J. Am. Chem. Soc.* **128,** 14020–14021 (2006).
17. Maye, M. M., Nykypanchuk, D., van der Lelie, D. & Gang, O. DNA-Regulated micro- and nanoparticle assembly. *Small* **3,** 1678–1682 (2007).
18. Park, S. J., Lazarides, A. A., Mirkin, C. A. & Letsinger, R. L. Directed assembly of periodic materials from protein and oligonucleotide-modified nanoparticle building blocks. *Angew. Chem. Int. Edn Engl.* **40,** 2909–2912 (2001).
19. Park, S. J., Lazarides, A. A., Storhoff, J. J., Pesce, L. & Mirkin, C. A. The structural characterization of oligonucleotide-modified gold nanoparticle networks formed by DNA hybridization. *J. Phys. Chem. B* **108,** 12375–12380 (2004).
20. Nykypanchuk, D., Maye, M. M., van der Lelie, D. & Gang, O. DNA-based approach for interparticle interaction control. *Langmuir* **23,** 6305–6314 (2007).
21. Valignat, M. P., Theodoly, O., Crocker, J. C., Russel, W. B. & Chaikin, P. M. Reversible self-assembly and directed assembly of DNA-linked micrometer-sized colloids. *Proc. Natl Acad. Sci. USA* **102,** 4225–4229 (2005).
22. Biancaniello, P. L., Kim, A. J. & Crocker, J. C. Colloidal interactions and self-assembly using DNA hybridization. *Phys. Rev. Lett.* **94,** 058302 (2005).
23. Rogers, P. H. *et al.* Selective, controllable, and reversible aggregation of polystyrene latex microspheres via DNA hybridization. *Langmuir* **21,** 5562–5569 (2005).
24. Israelachvili, J. N. *Intermolecular and Surface Forces* 2nd edn (Academic Press, London, 1992).
25. Milner, S. T. Compressing polymer brushes—a quantitative comparison of theory and experiment. *Europhys. Lett.* **7,** 695–699 (1988).
26. Warren, B. E. *X-ray Diffraction* Ch. 13 (Addison-Wesley, Reading, Massachusetts, 1969).
27. Dan, N. & Tirrell, M. Polymers tethered to curved interfaces—a self-consistent-field analysis. *Macromolecules* **25,** 2890–2895 (1992).
28. Rubinstein, M. & Colby, R. H. *Polymer Physics* Ch. 3 (Oxford Univ. Press, New York, 2003).
29. Lytton-Jean, A. K. R. & Mirkin, C. A. A thermodynamic investigation into the binding properties of DNA functionalized gold nanoparticle probes and molecular fluorophore probes. *J. Am. Chem. Soc.* **127,** 12754–12755 (2005).
30. Hurst, S. J., Lytton-Jean, A. K. R. & Mirkin, C. A. Maximizing DNA loading on a range of gold nanoparticle sizes. *Anal. Chem.* **78,** 8313–8318 (2006).

Supplementary Information is linked to the online version of the paper at www.nature.com/nature.

Acknowledgements We acknowledge the support of the Division Materials Science and Engineering in the Office of Basic Energy Sciences within the US DOE Office of Science. We thank the Center for Functional Nanomaterials and National Synchrotron Light Source at Brookhaven National Laboratory for the use of their facilities.

Author Contributions D.N., M.M.M., D.v.d.L. and O.G. contributed to the design of the experiment. M.M.M. synthesized and functionalized nanoparticles. D.N., M.M.M. and O.G. collected data and prepared the manuscript. D.N. processed X-ray data. O.G. directed the research.

Author Information Reprints and permissions information is available at www.nature.com/reprints. Correspondence and requests for materials should be addressed to O.G. (ogang@bnl.gov).